IEEE Instrumentation and Measurement
Technology Conference
St. Paul, Minnesota, USA, May 18-21, 1998

Characterization of a Neural Network-Based Trajectory Recognition Optical Sensor for an Automated Guided Vehicle

G.A. Borges, A.M.N. Lima and G.S. Deep
Laboratório de Instrumentação Eletrônica e Controle - LIEC
Departamento de Engenharia Elétrica - DEE
Universidade Federal da Paraíba - UFPB
Caixa Postal 10.004, Campina Grande, PB, 58109-970, Brazil
Phone: (+55)83.3101146, E-Mail: {geovany,marcus,deep}@dee.ufpb.br

Abstract— **Characterization of a relatively simple optical sensor system used for recognition of the desired fixed trajectory for an Automated Guided Vehicle, painted on an industrial shop floor, is described. The optical sensor consists of 14 IR emitter-detector pairs arranged in two columns and is fixed underneath the vehicle chassis. A microcomputer-based test platform for evaluation of the proposed sensor is also described. The sensor performance is evaluated using geometrical algorithms and one based on neural networks, latter giving much better results.**

Keywords— **Automated Guided Vehicles, Tracking System and Neural Networks**

I. Introduction

Automated Guided Vehicles (AGVs) are, in general, employed in an industrial environment to transport objects like tools, raw materials and manufactured items between different machines or production cells. In general, these vehicles move under supervised navigation employing an embedded control system and a remote supervising station. The desired path along which the vehicle should move, may be a fixed route, semi-fixed route or an arbitrary route, as described below [1]:

1. Fixed route implies the installation of a fixed active guide like an energized cable or a passive one like a reflecting strip painted on the plant floor. The main problem with fixed route guide is the physical restriction on its installation (e.g. minimum curvature ratio must be respected), because in most cases is not possible to move a machine from its current position to give place to the route guide.

2. A semi-fixed route may be specified by some markings at strategic locations, like bar codes, magnets or some other type of artificial landmarks [2], [3]. One of the methods used with the semifixed route configuration employs a low precision odometer and a sensor scheme to identify a prespecified marking or other landmark. During the motion of the vehicle between two markings, the navigation system updates the absolute position of the vehicle based on the odometer reading and this absolute position is further corrected when a specified marking is identified. In this scheme, the distance between two consecutive markings needs to be limited so that the odometer reading can be relied upon.

3. Arbitrary routes require the use of more complex position determination techniques such like GPS (Global Positioning System), recognition of the surrounding by image processing, use of gyroscope, sonar, laser beacon or map-based position detection [2], [4], [5], [6], [7], [8], [9]. These are used to determine the absolute position of the vehicle. For a known surrounding, map comparison is used, and it is aided by one or more methods of recognition of the surrounding like sonar, laser beacons and video cameras. The vehicles used for following an arbitrary route should have some autonomy in the choice of the track and such vehicles are termed as autonomous vehicles.

In the recent past, some techniques for the navigation of the AGVs on industrial shop floors or elsewhere [10], [11], based on one of the above three options, have been presented. The authors have not come across a general solution and for a particular type of surrounding and a given application, one or the other option may be found more suitable.

In this paper, the emphasis is on the characterization of an optical sensor scheme for guiding a vehicle along a prefixed route, in the form of a painted trajectory on a shop floor. Some configurations for the navigation of a vehicle along a fixed painted trajectory have been reported in literature [12], [13]. In [12], six infrared emitter-detectors pairs are employed. The number of IR detectors not covered by the painted trajectory is employed for the nonlinear control scheme for keeping the vehicle within close tolerances of trajectory by controlling the speed of the differential traction motors. In [13], a more complex scheme is proposed. It is based on a CCD video camera and an image acquisition card sitting in the expansion slot of a PC, to image the trajectory and for direct determination of the variables, characteristic of the deviation of the vehicle from the desired trajectory. This deviation was quantified in terms of number of pixels for empirically chosen variables from the geometrical formulation of the acquired image. With a video camera of a reason-

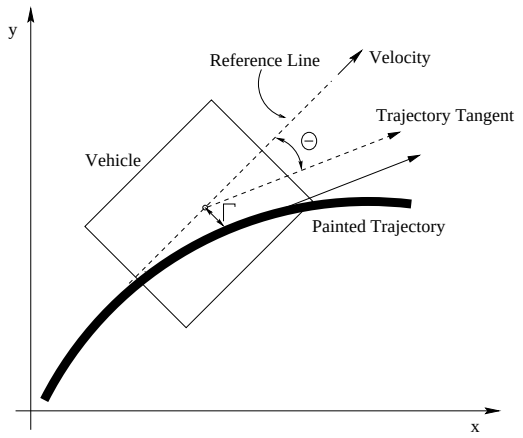

Fig. 1. Trajectory error variables characterization.

able resolution, the estimates of the trajectory deviation variables were considered good. The cost of such a system is on the higher side and the sampling rate is rather low due to the relatively large time spent in the acquisition and processing of the image.

II. Proposed System

A prototype AGV is being assembled in our laboratory and is designed to track a fixed route. An optical marking in the form of a strip painted on the floor is the route guide or the desired trajectory. The color of the painted strip contrasts against that of the floor. In the experimental system, the route guide is painted black on the white floor. The objective of the navigation control of the AGV is to keep the vehicle along the painted route guide, during its motion [14]. In any case it is necessary to measure the vehicle's deviation from the trajectory. As shown in Fig. 1, the two variables, the angular deviation Θ and the orthogonal displacement Γ, quantify the difference between the painted trajectory and the actual path of the vehicle at a given instant. The navigation system of the prototype vehicle consists of three units: the image acquisition unit (IAU), the image processing unit (IPU) and the trajectory control unit (TCU).

The determination of the vehicle deviation with respect to the route guide is usually done by processing the image acquired by optical sensor like a CCD camera. In our prototype, the vehicle deviation is estimated from the data acquired by an array of infrared (IR) emitter and detector pairs arranged in two columns, fixed underneath the vehicle chassis. This array together with a signal conditioning circuit for each detector constitutes the IAU. The optical sensor is configured as shown in Fig. 2(a). The width of the painted trajectory should be equal to the spacing between two consecutive detector. For the arrangement shown in Fig. 2(a), the hypothetical sensor reference line is the one that connects the detectors numbers 4 and 11. For consistent data, the route guide should always lie below both the IR detector columns. In Fig. 2(b) the schematic of the IAU fixed under the chassis of the vehicle and placed just above the painted route guide

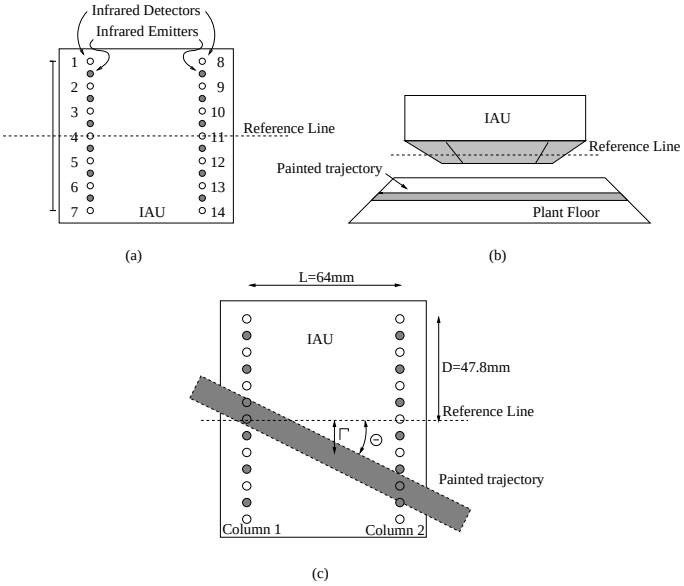

Fig. 2. (a) The schematic of the optical sensors (Image Acquisition Unit - IAU) with infrared emitters and detectors. (b) The relative position of the Image Acquisition Unit with respect to the plant floor. (c) defining the vehicle position with respect to the painted trajectory.

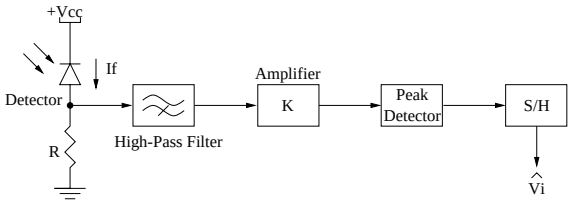

Fig. 3. Block diagram of the signal conditioning circuitry of each detector in the IAU.

is shown. In Fig. 2(c) the variables Θ and Γ are depicted to quantify the deviation of the vehicle from the painted trajectory, for an arbitrary position of the AGV.

The IR detectors receive a radiation pulse reflected from the shop floor when the emitters are excited by a pulsed current (pulse width $\approx 100\mu s$). The radiation intensity incident on the detector depends upon whether the detector is just above the painted route guide or not. The reverse biased IR detector output is connected to a signal conditioning circuit as shown in Fig. 3, and the magnitude of the output voltage is directly proportional to the amount of energy received. There are 14 such circuits corresponding to 14 IR detectors used in the sensor scheme, and $\hat{V}_i$ $(i = 1 \ldots 14)$ is the output voltage related to the i^{th} detector conditioning circuit. Thus a 14 element column vector with these 14 values of $\hat{V}_i$ is termed as a image vector for a given position of the vehicle with respect to the painted trajectory.

The main task of the proposed system is the estimation of trajectory deviation variables in the image processing unit (IPU).

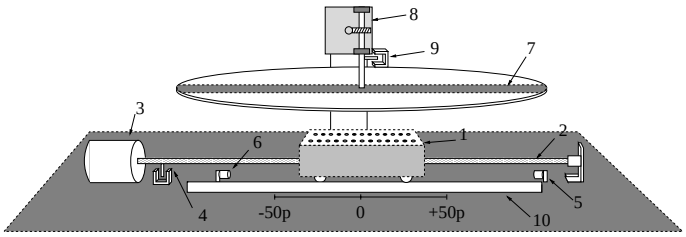

Fig. 4. Schematic of the sensor test-platform.

III. Laboratory Test Platform

In order to characterize the proposed sensor an experimental test platform was constructed in the laboratory to simulate the deviation of the vehicle from a painted route guide during its movement. This platform consists of a movable disk (diameter of $330mm$) mounted on a vertical shaft coupled to a stepping motor, as shown in Fig. 4. This disk, with a painted strip underneath, corresponds to the floor. The disk is displaced to simulate an angular deviation Θ of the sensor with respect to the desired trajectory. The sensor mounted on a motorized leadscrew is displaced to independently impose the orthogonal displacement Γ from the painted route guide. The leadscrew is rotated by a 24 step stepping motor, and one revolution of the leadscrew corresponds to a linear displacement of $p = 1.56mm$ (designated as one step of the linear motion of the sensor) of the sensor position. The optical sensor (4) is used to count the number of revolutions of the leadscrew. The limit switches (5) and (6) are used to indicate the limit of the linear movement of the sensor restricted to 101 steps ($-50p$ to $+50p$), equivalent to $156mm$. A valid test point in this platform is obtained when the painted guide route covers at least two IR detectors, one in each column. For a given orthogonal displacement Γ, the maximum angle of the rotating disk is limited to $\Theta_{\max}$, given by

$$\Theta_{\max} = \tan^{-1}\left(\frac{D - |\Gamma|}{L/2}\right), \qquad (1)$$

where D and L are physical dimensions of the image sensor (Fig. 2(c)). The maximum value of $\Theta_{\max}$ is 56.20^o, obtained when $\Gamma = 0$.

This yields a maximum of $5,365$ valid test points which can be obtained in this test assembly. The angular deviation can be varied between $-\pi$ to $+\pi$ with a resolution of 0.0131rad, or 0.75^o.

The output voltages $\hat{V}_i$ of the conditioning circuits associated with the IR detectors (as shown in Fig. 3) are multiplexed and digitized in an 8 bit A/D converter. The A/D converter output is fed to a PC through its parallel port. This parallel port is also used to send commands to the stepping motors in the test platform and sense the outputs of the limit switches. Under software control, we can position the rotating disk (7) and the IAU (1) to generate different image vectors $\mathbf{X}$ for given deviation variables pair (Θ, Γ). Each image vector is stored in a disk file in the form $(\Theta, \Gamma, \mathbf{X})$. The image vector $\mathbf{X}$ may be written as

$$\mathbf{X} = \left[\ x_1 \quad x_2 \quad \ldots \quad x_i \quad \ldots \quad x_{14}\ \right]^{\mathbf{T}}, \qquad (2)$$

where x_i is the digital value of the output voltage $\hat{V}_i$ of the i^{th} sensor conditioning circuit. A specific normalizing image vector $\mathbf{X_n}$ is obtained when all the 14 emitter-detector pairs of the sensor are away from the painted trajectory (Fig. 4). The elements of the $\mathbf{X_n}$ vector have the maximum obtainable values.

IV. Γ and Θ estimation

The estimates of Γ and Θ ($\hat{\Gamma}$ and $\hat{\Theta}$ respectively) of the trajectory deviation variables are obtained from IPU, by using an estimation algorithm. There are different methods to obtain these estimates but in this paper we shall describe straightforward geometrical techniques and a neural network based technique. These techniques were evaluated experimentally in the test platform.

A. Geometrical algorithms

Vehicle deviation estimation algorithms based on geometrical formulations of the image have been employed with high resolution cameras for imaging the fixed route guide. In the case of low resolution imaging devices, these algorithms may introduce unacceptable errors. For the sensor being discussed we propose two geometrical algorithms. These algorithms employ a normalized position index associated with each of 14 IR detectors.

A.1 Algorithm A

The two normalized position indices p_1 and p_2 refer to the detectors in column 1 and 2 respectively. These indice are related with the IR detector l with the lowest radiation on it (minimum output voltage of the conditioning circuit associated with this detector), which occurs when the detector is just above the painted route guide in an actual vehicle prototype (below in the case of the laboratory test platform). In Fig. 2(c) the sensor numbers 4 (column 1) and 13 (column 2) are just below (in the test platform) the route guide painted on the movable disk. The normalized position indices are defined as

$$p_1(l) = \frac{l-4}{3}\ , \text{for } l = 1, \ldots, 7, \qquad (3)$$

$$p_2(l) = \frac{l-11}{3}, \text{for } l = 8, \ldots, 14, \qquad (4)$$

and thus

$$-1 \le p_1(l) \le 1, \forall l,$$
$$-1 \le p_2(l) \le 1, \forall l.$$

These normalized indice represent a measure of the distance of sensor l from the reference line. The dimensions L and D (see Fig. 2(c)) are in units of linear displacement step (p) of the sensor assembly corresponding to one revolution of the leadscrew. The absolute value of the step p is 1.56mm. Thus the orthogonal distance Γ of the sensor l in column 1 from sensor's reference line is given by $p_1(l)\mathrm{x}D$.

Its relatively easy to show that $\hat{\Gamma}$ and $\hat{\Theta}$ are given by

$$\hat{\Gamma} = \frac{P_1 + P_2}{2} D, \qquad (5)$$

$$\hat{\theta} = \arctan\left(\frac{P_2 - P_1}{L} D\right), \qquad (6)$$

where $P_1 = p_1(l)$ with l being the sensor number in column 1 which is just below the route guide and $P_2 = p_2(l)$ for the corresponding sensor in column 2.

In this algorithm, once the IR detectors with the least or null radiation in each column have been identified, the position indice are determined as per equations (3) and (4) and the trajectory deviation variables $\hat{\Gamma}$ and $\hat{\theta}$ are calculated using equations (5) and (6). However, this algorithm does not give good estimates of Θ and Γ when the route guide covers partially two adjacent IR detectors in the same column.

A.2 Algorithm B

To get meaningful results and accommodate the cases where the route guide partially covers two adjacent detectors, the equivalent sensor number l (as in equations (3) and (4)) can be calculated as the weighted mean of the two sensor positions l_A and l_B (associated with the partially covered sensors). The weighting factors associated with the sensors l_A and l_B are based on the normalized entries in the image vector, i.e., x_A/x_{An} and x_B/x_{Bn}, respectively. Thus the equivalent sensor number to be used in equations (3) and (4) will be given by

$$l = \frac{l_A(1 - x_A/x_{An}) + l_B(1 - x_B/x_{Bn})}{(1 - x_A/x_{An}) + (1 - x_B/x_{Bn})}, \qquad (7)$$

where x_{An} and x_{Bn} are the normalizing radiation intensities for the sensors l_A and l_B. It is interesting to observe that the weighting factors used in equation (7) have the following characteristics (for the test platform): $1 - x_A/x_{An} \approx 1$ if the route guide is above the detector l_A, and $1 - x_A/x_{An} \approx 0$ if the route guide is not above the detector l_A.

B. Neural Networks-Based Estimation

The estimation of the vehicle position deviation in terms of $\hat{\Gamma}$ and $\hat{\theta}$ with respect to the painted route guide may be done using two artificial neural networks (ANNs), one for $\hat{\Gamma}$ and another for $\hat{\theta}$. The input to each of the ANNs are the 14 IR detector conditioning circuit output voltages. The neural networks are forward multi-layer perceptron type and implement identification of a nonlinear model. These employ nonlinear neurons in the hidden layer and linear output neurons [15], [16], [17], [18]. This implementation provides global approximations or generalizations of the input patterns not used during the training phase. These generalizations are desirable once we recognize that we have a limited number of valid test points due to the discrete nature of positioning procedure employed in the test platform.

Both the ANNs contain three layers as shown in Fig. 5. The input layer contains 14 elements that correspond to the dimension of image vector $\mathbf{X}$ (14 IR detectors). The entries in the image vector are normalized relative to the maximum possible output of each of the IR detector

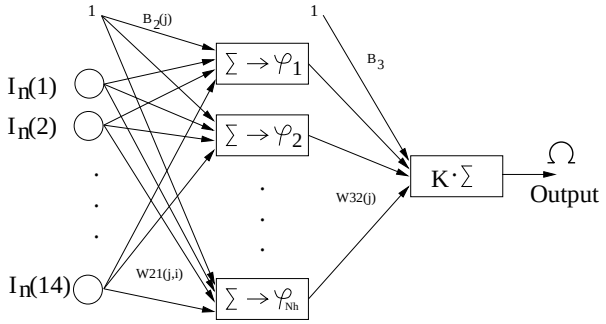

Fig. 5. Structure of the Neural Networks employed for estimation of vehicle deviation variables.

conditioning circuits as contained in the $\mathbf{X_n}$ vector. This normalization consists in dividing each element of the image vector by its corresponding entry in the normalizing vector X_n and subtracting 0.5 from the quotient. Thus, the normalized input vector $\mathbf{I_n}$ for each neural network is given by

$$\mathbf{I_n} = \left[\begin{array}{ccc} \frac{\mathbf{X(1)}}{\mathbf{X_n(1)}} - 0.5 & \ldots & \frac{\mathbf{X(14)}}{\mathbf{X_n(14)}} - 0.5 \end{array} \right]^{\mathbf{T}}. \qquad (8)$$

The hidden layer dimension (N_h) is determined after some experimentation with different number of neurons in the hidden layer. The activation potentials of the j^{th} neuron of the hidden layer is given by

$$v_j = B_2(j) + \sum_{i=1}^{14} \mathbf{I_n(i)} \mathbf{W_{21}(j,i)}, \qquad (9)$$

where $B_2(j)$ is the bias of the j^{th} neuron and $W_{21}(j,i)$ is the synaptic weight related to the i^{th} input of the j^{th} neuron in the hidden layer.

The activation function for the j^{th} neuron is given as

$$\varphi_j(v_j) = \sigma_j \frac{1 - \exp(-\beta_j v_j + \alpha_j)}{1 + \exp(-\beta_j v_j + \alpha_j)} \text{ for } j = 1, \cdots, N_h. \qquad (10)$$

The output layer contains only one neuron with output given as

$$\Omega = K \left[B_3 + \sum_{j=1}^{N_h} \varphi_j(v_j) W_{32}(j) \right], \qquad (11)$$

where B_3 is the bias and $W_{32}(j)$ is the weighting factor related with the j^{th} input of the output neuron. As the output Ω of the neural network depends upon the image vector $\mathbf{X}$, one may specify the neural network output as $\Omega(\mathbf{X})$.

B.1 Training of ANNs

The training of neural networks is done to enable them to perform a nonlinear mapping procedure. The training is based on back-propagation algorithm in which Newton's steepest descent method is employed for adjusting the weighting factors W_{21}, W_{32}, B_2 and B_3. The same method is employed to adjust the parameters α_j, β_j and σ_j of the j^{th} neuron activation function as given in equation (10).

A total of 750 (N_t) randomly chosen training positions (Θ_q, Γ_q) for the two neural networks were employed in the test platform ($q = 1, 2, \ldots, 750$). The corresponding image vectors $\mathbf{X_q}$ were monitored. The objective of the training phase is to minimize the cost functions J_Θ and J_Γ defined as

$$J_\Theta = \frac{1}{2N_t}\sum_{q=1}^{N_t}(\Theta_q - \hat{\Theta}_q)^2, \quad (12)$$

$$J_\Gamma = \frac{1}{2N_t}\sum_{q=1}^{N_t}(\Gamma_q - \hat{\Gamma}_q)^2, \quad (13)$$

where $\hat{\Theta}_q = \Omega_\Theta(\mathbf{X_q})$ and $\hat{\Gamma}_q = \Omega_\Gamma(\mathbf{X_q})$ are the outputs of the ANNs used for estimation of Θ and Γ, respectively, for a given image vector input $\mathbf{X_q}$.

Some experiments with different number of neurons (N_h = 4, 7, 14 and 28) in the hidden layer for Γ and θ estimation ANNs were conducted. 400 training epochs, each employing all the 750 training points in a random order, were conducted. The random ordering of the training data was done to avoid local minimums for the cost functions J_Θ and J_Γ [15].

An additional 400 positions different from those used during the training phase were used to verify the effectiveness of the training procedure. Using cost functions similar to equations (12) and (13) for these positions, it was found that $N_h = 4$ for Γ estimation ANN and $N_h = 7$ for Θ estimation gave acceptable performances. The evolution of the cost functions during the training phase demonstrated that about 250 training epochs for the Θ estimation ANN and 50 training epochs for the Γ estimation ANN, are sufficient for the off-line training get the cost functions $J_\Theta = 3.2382$ and $J_\Gamma = 1.7733$.

V. Experimental Validation

The performance of the IPU algorithms was experimentally evaluated by sinusoidally varying the orthogonal displacement Γ and cosinusoidally varying the angular deviation Θ of the disk in the test platform, by appropriately commanding the two stepper motors. The i^{th} validation pair (Θ_i, Γ_i) was generated according to the following equations:

$$\Gamma_i = 20\sin(\frac{2\pi i}{400}), \quad (14)$$

$$\Theta_i = 30\cos(\frac{2\pi i}{400}), \quad (15)$$

with $i = 1 \ldots 400$.

These test results for the estimates of Γ_i and Θ_i employing the three algorithms are shown in Fig. 6, 7 and 8. The solid line plots represent the imposed values of Γ_i and Θ_i and the discontinuous line plots represent the estimated values.

Again, cost functions similar to ones given by (12) and (13) were used to evaluate the performance of the trained neural networks and the geometrical algorithms A and B.

The values of J_Γ and J_Θ as obtained during the experiments with the test platform are given in table I.

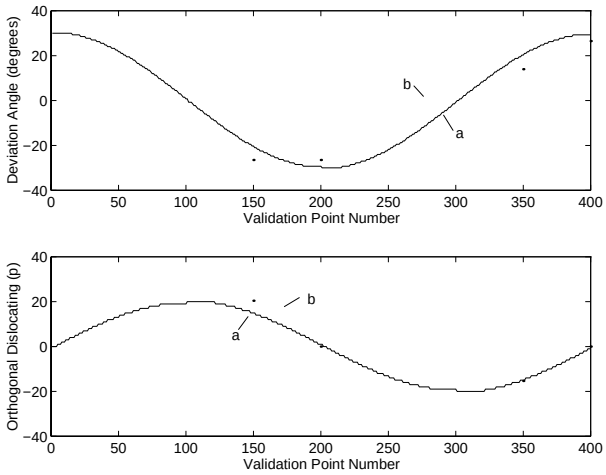

Fig. 6. Validation experiment results of trajectory tracking for the Algorithm A. (a) Imposed trajectory. (b) Estimated trajectory.

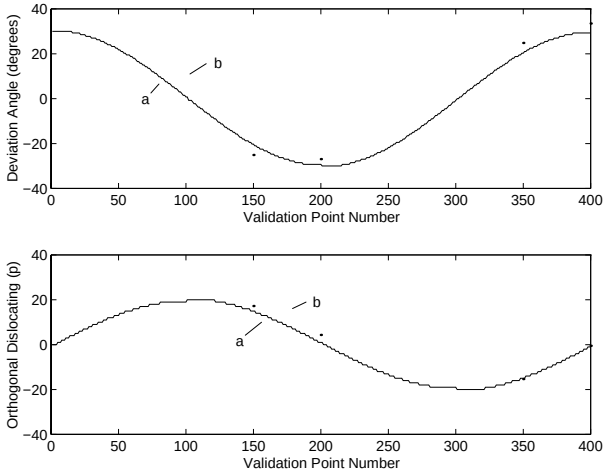

Fig. 7. Validation experiment results of trajectory tracking for the Algorithm B. (a) Imposed trajectory. (b) Estimated trajectory.

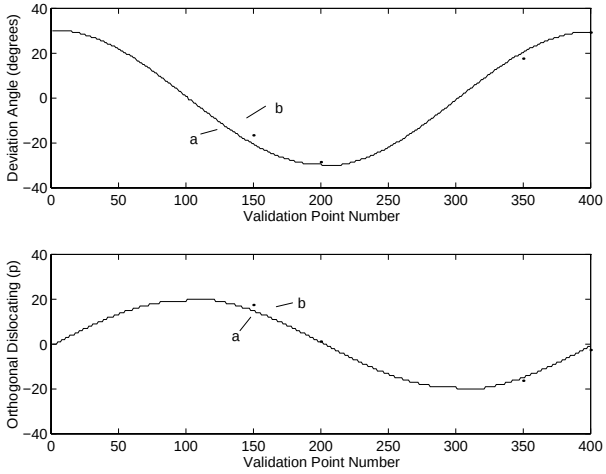

Fig. 8. Validation experiment results of trajectory tracking for the Neural Networks. (a) Imposed trajectory. (b) Estimated trajectory.

TABLE I

Validation cost function values for different algorithms.

Algorithm	J_Θ	J_Γ
Algorithm A	21.311	6.049
Algorithm B	7.601	3.030
Neural Network	4.280	1.941

TABLE II

Processing times for different phases of the system.

Processing Phase	**Time Required**
Image Acquisition	$3.0ms$
Algorithm A	$116\mu s$
Algorithm B	$236\mu s$
Neural Networks	$240\mu s$

VI. Comparison of the three methods

From table I, we observe that the use of ANNs for Θ and Γ estimation has given lowest values of the cost functions. Besides the performance curve of the ANNs (Fig. 8) are much smoother than those of the geometrical algorithms (Fig. 6 and 7). The smoothness of the curve in Fig. 8 is an advantage for a trajectory controller with large sensitivity at higher frequencies.

Another aspect in the comparison of the three methods is the time spent in getting the final values of the $\hat{\Theta}$ and $\hat{\Gamma}$ estimates. This time is made up of two phases namely the image acquisition phase and the image processing phase. The image acquisition phase is the same for all the three methods, but the processing time is different for the three algorithms, and these are given in table II. These times are based on the use of a 100Mhz Pentium PC. The image processing time is quite small compared to the time for the acquisition of the image. The image acquisition time is relatively large due to the type of A/D converter employed in the prototype, which can be reduced by a factor of 10 using a faster A/D converter.

VII. Conclusions

A laboratory test platform for characterizing an optical sensor system proposed for quantifying the deviation of an automated guided vehicle from a fixed trajectory has been described. Three different methods for estimating the vehicle deviation variables Θ and Γ were evaluated. The ANN-based method has demonstrated much better results compared to the geometrical formulations although it takes more time for processing the acquired image. The ANN-based algorithm has demonstrated hardly any discontinuity in $\hat{\Theta}$ and $\hat{\Gamma}$ estimate curves offering an advantage in the vehicle trajectory controller design and operations. It is proposed to replace the two ANNs for Θ and Γ estimates by only one ANN with two outputs. This should further reduce the image processing time.

Acknowledgment

The authors thank the CNPq (Conselho Nacional de Desenvolvimento Científico e Tecnológico) for the award of research and study fellowships during the course of these investigations.

References

[1] P.E. Miyagi, J.C. Adamowski, L.A. Moscato, J. Okamoto, and M.R.P. Barretto, "Veículos autônomos de transporte e seus controles," in *III Congresso Nacional de Automação Industrial*, September 1988, pp. 226–233.

[2] Johann Borenstein, H.R. Everett, and Liqiang Feng, *Navigating Mobile Robots - Systems and Techniques*, AK Peters, 1996.

[3] Takero Hongo, Hideo Arakawa, Gunji Sugimoto, Koichi Tange, and Yuzo Yamamoto, "An automatic guidance system of a self-controlled vehicle," *IEEE Transactions on Industrial Electronics*, vol. 34, no. 1, pp. 5–10, February 1987.

[4] Raimo Ahola and Risto Myllyla, "A time-of-flight laser receiver for moving objects," *IEEE Transactions on Instrumentation and Measurement*, vol. 35, no. 2, pp. 216–222, June 1986.

[5] Ingemar J. Cox, "Blanche - an experiment in guidance and navigation of an autonomous robot vehicle," *IEEE Transactions on Robotics and Automation*, vol. 7, no. 2, pp. 193–204, April 1991.

[6] Larry Korba, Shadia Elgazzar, and Timothy Welch, "Active infrared sensors for mobile robots," *IEEE Transactions on Industrial Electronics*, vol. 43, no. 2, pp. 283–287, April 1994.

[7] Andreas Kurz, "Constructing maps for mobile robot navigation based on ultrasonic range data," *IEEE Transactions on Systems, Man and Cybernetics*, vol. 26, no. 2, pp. 233–242, April 1996.

[8] Daniele Marioli, Emilio Sardini, and Andrea Taroni, "Ultrasonic distance measurement for linear and angular position control," *IEEE Transactions on Instrumentation and Measurement*, vol. 37, no. 4, pp. 578–582, December 1988.

[9] Won Soo Yun, Dong Woo Cho, and Yoon Su Baek, "Dynamic path planning for robot navigation using sonar mapping and neural networks," *IEE Journal of Dynamic Systems, Measurement and Control*, vol. 119, pp. 19–26, March 1997.

[10] R. Andrew Russel, "Laying and sensing odor markings as a strategy for assisting mobile robot navigation tasks," *Robotics and Automation Magazine*, pp. 3–9, 1995.

[11] Hans W. Wehn and Pierre R. Bélanger, "Ultrasound-based robot position estimation," *IEEE Transactions on Robotics and Automation*, vol. 13, no. 5, pp. 682–692, October 1997.

[12] Eric Sung, Ng Kok Loon, and Yee Chiang Yin, "Parallel linkage steering for an automated guided vehicle," *IEEE Control Systems Magazine*, pp. 3–8, 1989.

[13] Elder M. Hemerly and Cláudio C. Rodrigues, "Guiagem de veículos autônomos utilizando sensor de visão," in *Conf. Rec. CBA*, September 1994, pp. 873–878.

[14] Geovany Araújo Borges and Antonio Marcus Nogueira Lima, "Sistema óptico de reconhecimento de trajetória para veículos autônomos utilizando redes neurais," in *III Congresso Brasileiro de Redes Neurais*, July 1997, pp. 414–418.

[15] Simon Haykin, *Neural Networks - A Comprehensive Foundation*, Prentice Hall, 1994.

[16] J. Sjöberg, *Non-Linear System Identification with Neural Networks*, Ph.D. thesis, Linköping University, 1995.

[17] L. Ljung and J. Söberg, "A system identification perspective on neural nets," Tech. Rep., Linköping University, 1992.

[18] J. Sjöberg, H. Hjalmarsson, and L. Ljung, "Neural networks in system identification," Tech. Rep., Linköping University, 1993.